PAPER

Check for updates

Electrochemical quantification of phosphonic acid passivated surface sites of NiO$_x$ for perovskite solar cells

Chenchao Xie, [ID] [a] Duong Nguyen Minh,[a] Rita Kret, [ID] [a] Jacob Hoffman,[b] Angelo P. Rillera,[c] Regan G. Wilks, [ID] [cd] Roberto Félix, [ID] [c] Michael A. Anderson,[c] Johannes Frisch,[cd] Marcus Bär, [ID] [cdef] Marc Migliozzi,[a] Amy Louks,[ag] Kelly Schutt, [ID] [a] Lance M. Wheeler, [ID] [a] Joseph J. Berry,[ahi] Kai Zhu, [ID] [a] Ross A. Kerner [ID] *[a] and Joseph M. Luther [ID] *[a]

Nickel oxide (NiO$_x$) is among the few p-type metal oxide semiconductors considered a strong candidate for hole transport layers in halide perovskite solar cells (PSCs). However, its reactivity with perovskite ions poses significant challenges to achieving high efficiency and long-term stability. Here, we investigate passivation of detrimental reactive surface sites on NiO$_x$ by carbazole phosphonic acids. We leverage electrochemical cyclic voltammetry (CV) of NiO$_x$ electrodes as a *proxy measure* for the redox activity that afflicts PSCs. From the CVs, we derive a metric, N (units cm^{-2}), that relates to the number of redox active sites on NiO$_x$ surfaces. We observe a statistically significant negative correlation between PSC efficiency and N-value that indicates PSCs are more efficient on NiO$_x$ with lower electrochemical reactivity. The new mechanistic insight into NiO$_x$ passivation demonstrates it requires a reducing agent and Brønsted acid combination, providing a broadly applicable approach for evaluating and enhancing the stability and performance of NiO$_x$-based interfaces in photovoltaics.

Broader context

Nickel oxide (NiO$_x$), a widely used hole transport layer in perovskite solar cells (PSCs), plays a critical role in device performance but often suffers from interfacial reactivity with perovskite ions, leading to degradation and instability. Although PSCs are considered leading candidates for next-generation photovoltaics due to their high efficiency, solution processability, and low manufacturing costs, their long-term stability remains a major obstacle to commercialization. In this work, we introduce a straightforward electrochemical method—integrated cyclic voltammetry—to directly count redox-active surface sites and quantify this interfacial reactivity. By attaching carbazole or other phosphonic acid molecules directly to these reactive sites to suppress the number, we demonstrate improvements in both efficiency and stability. More broadly, our study establishes a general framework for diagnosing and mitigating detrimental surface reactivity in metal oxide–based interfaces, offering design principles for robust, high-performance energy conversion technologies.

[a] *National Laboratory of the Rockies, Golden, Colorado, 80401, USA.*
 E-mail: Ross.Kerner@nrel.gov, Joey.Luther@nrel.gov
[b] *Cubic PV Co., Ltd, Bedford, MA, 01730, USA*
[c] *Department Interface Design, Helmholtz-Zentrum Berlin für Materialien und Energie GmbH, Berlin, Germany*
[d] *Energy Materials In-Situ Laboratory Berlin (EMIL), Helmholtz-Zentrum Berlin für Materialien und Energie GmbH, Berlin, Germany*
[e] *Department of Chemistry and Pharmacy, Friedrich-Alexander-Universität Erlangen-Nürnberg, Erlangen, Germany*
[f] *Department for X-ray Spectroscopy at Interfaces of Thin Films, Helmholtz-Institute Erlangen-Nürnberg for Renewable Energy (HI ERN), Berlin, Germany*
[g] *Chemistry Department, Colorado School of Mines, Golden, Colorado, 80401, USA*
[h] *Physics Department, University of Colorado, Boulder, Colorado, 80303, USA*
[i] *Renewable and Sustainable Energy Institute (RASEI), University of Colorado, Boulder, 80303, USA*

Introduction

Cubic phase nickel oxide (NiO), often denoted NiO$_x$ to represent deviations from ideal stoichiometry and OH groups, where the H is implicit. It is well-known to have p-type semiconducting character with a relatively shallow valence band maximum (VBM) and ionization energy ranging from 3.9–5.7 eV.[1–3] It is therefore a viable candidate as a hole collection contact in photovoltaic devices[4,5] such as metal halide perovskite solar cells (PSCs)[6–9] and a low resistance hole injection contact in transistors,[10] light-emitting diodes,[11] and sensors.[12,13] Because it is an oxide, it is potentially more stable at elevated temperatures in combination with illumination where organic molecules might experience rapid degradation.[14–17] Therefore, it is a

promising candidate to improve device durability for PSC commercialization. However, a significant issue lies in chemical reactions at interfaces between NiO_x and the halide perovskite material, specifically in its tendency to degrade iodide anions and organic cations in the perovskite structure as previously reported.[7,18–21] In extreme cases, NiO_x can react with perovskite salts like methylammonium iodide (MAI) to convert to NiI_2.[20,21] These degradation reactions are a major obstacle to device efficiency and longevity.[22]

A significant contributing factor to instability of NiO_x/perovskite interfaces is the heterogeneous nature of the surface, which can exhibit multiple oxidation states, including Ni in the 2+, 3+, and even 4+ oxidation states.[23] Ni oxidation states $>2+$ are capable of oxidizing iodide, degrading methylammonium (MA) and formamidinium (FA) cations in the process.[7] Depending on the specific synthesis and processing methods used to prepare the NiO_x layer, the distribution of oxidation states and associated surface structures can differ widely, resulting in inconsistent PSC efficiency and stability.[23–25] This unpredictability should be better understood to enable reliable HTL materials in PSCs.[26,27] Often, the NiO_x surface can be passivated to improve PSC efficiency. While many passivation strategies exist, a commonly employed treatment is deposition of a carbazole (Cz) tethered to a phosphonic acid (PA) abbreviated as PACz. However, the mechanism by which the PACz "self-assembled monolayer" (SAM) passivates the NiO_x surface, and insight into how to design better passivation strategies, remains poorly understood.

In this study, we explore a representative set of PACz molecules with varying side groups at the Cz 3,6 positions and N-alkyl chain length between the Cz and PA to systematically understand the passivation efficacy. We find a clear correlation between the surface reactivity of NiO_x and the efficiency of resulting PSCs. Specifically, we utilize cyclic voltammetry (CV) in an aqueous KCl electrolyte to characterize the current density arising from reduction/oxidation (redox) of near surface ions and reactive ion adsorption sites at the NiO_x surface. We hypothesize that these active sites contribute directly to chemical reactions that result in detrimental defects during PSC device fabrication and operation. This rapid and inexpensive measurement acts as an excellent proxy for the types or extent of redox reactions one might expect at the NiO_x/perovskite interface. The PACz passivation is observed to suppress the redox activity and/or block surface sites for ion adsorption/reactions. We additionally derive a metric, N, to quantify the NiO_x surface reactivity by integrating the current density over an appropriate potential range. N is essentially proportional to a combination of surface and near surface redox reactions involving $Ni^{2+/3+}$ oxidation state changes, adsorption/desorption, and O/OH protonation/deprotonation.[7,28–30] In general, we believe N and electrochemical activity at NiO_x surfaces and interfaces should be minimized for optimal PSC efficiency.

We verify this hypothesis by fabricating PSCs from the NiO_x/PACz combinations and correlating the N-values to the PSC current density–voltage (J–V) parameters. The power conversion

efficiency (PCE) shows a strong and statistically significant negative correlation to the magnitude of current passed in the CV measurement. Our results reveal that passivation with PACzs decreases the number of reactive surface sites with differing efficacy, leading to a marked improvements in device efficiency with decreased N. This demonstrates the relevance of this measurement and its usefulness for accelerating PSC research and development for NiO_x-based devices. We envision that further work in this area could result in a rapid measurement capable of predicting PCE and are optimistic about future work correlating to stability.

Moreover, we apply the same experiment to simple alkyl phosphonic acids to decouple the role of the Cz and the PA to better understand the passivation reaction mechanism. The alkyl PAs show limited ability to passivate NiO_x and minimal improvement to PSC efficiency. Additional experiments on the ability of NiO_x to oxidize Czs reveal that effective passivation requires a combination of a reducing agent and a Brønsted acid (proton source). Finally, we briefly discuss broader implications, including relating to recent organic photovoltaic (OPV) observations where trends appear consistent with our results. This study provides a comprehensive, general strategy, and evaluation protocol for targeted surface passivation that decreases the reactivity of NiO_x for PSCs. Our findings go beyond conventional approaches to interface engineering in perovskite photovoltaics and offer rational design criteria based on data driven insights for the development of future materials and device architectures.

Result and discussion

Overview of NiO_x chemical properties

The ideal semiconductor phase is pure cubic, near stoichiometric NiO_x (Fig. 1a). Some defects are required to improve the hole conductivity. However, there are additionally many related Ni oxyhydroxide phases previously characterized and classified as α-$Ni(OH)_2$, β-$Ni(OH)_2$, β-NiOOH, and γ-NiOOH.[23,31,32] It is important to note that these phases are not pure and can contain mixtures of phases and oxidation states of Ni as well as varying amounts of intercalated species. In addition, a Ni_2O_3 phase exists, though it is challenging to isolate and characterize.[33,34] Moreover, a NiO_2 phase is theoretically feasible, but it is not expected to be stable since highly oxidizing Ni^{4+} will readily react with atmospheric water to form peroxides and partially reduce Ni^{4+} to Ni^{3+}, especially at surfaces.[35] The properties of NiO_x materials are sensitive to the synthetic conditions. For example, one researcher's β-NiOOH could have significantly different behavior than another's (Fig. 1b).

To complicate the surface chemistry more, the surface of NiO_x can have specifically adsorbed species such as hydroxides and peroxides (Fig. 1a). The surface termination, Ni oxidation state, and phases present are easily altered at low temperatures under changing conditions. For example, the surface will change when placed in a protic or hydrous environment and when voltages are applied, where cyclic voltage stressing can

This journal is © The Royal Society of Chemistry 2026

Energy Environ. Sci., 2026, **19**, 884–895 | 885
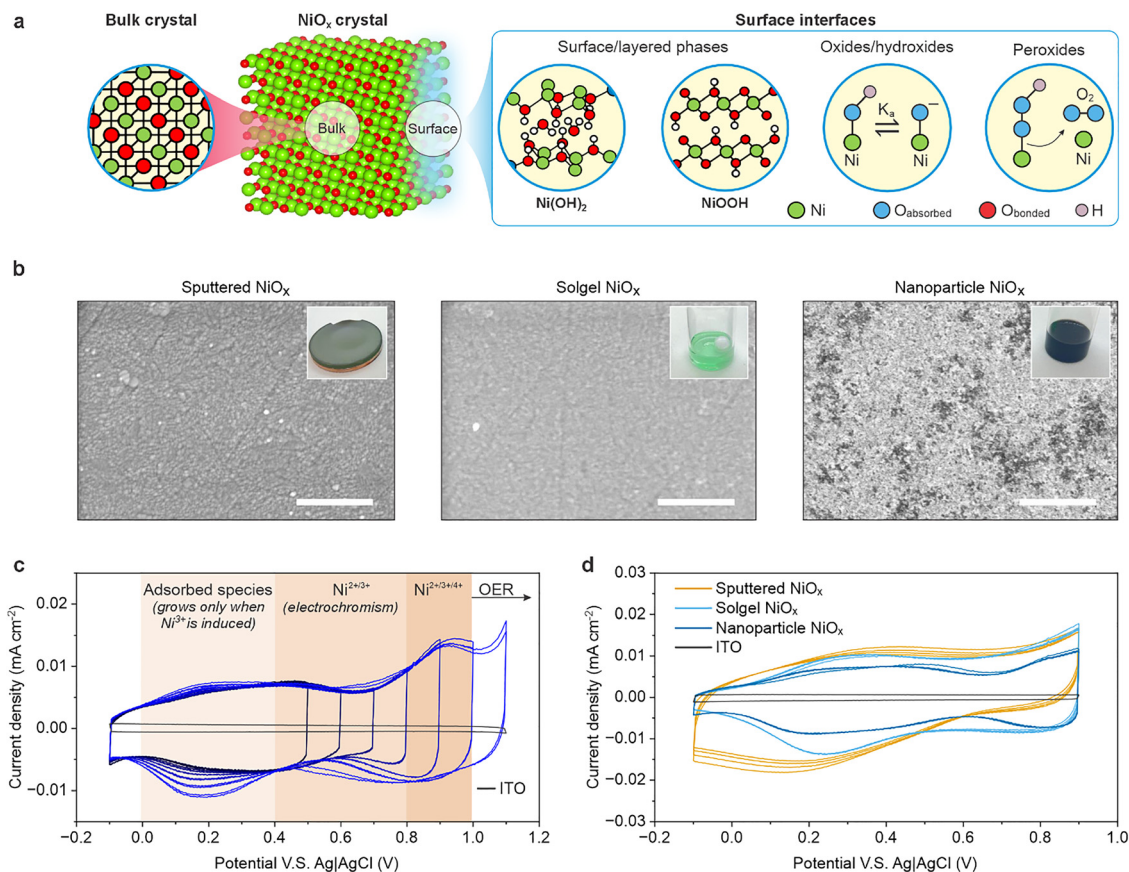
Fig. 1 NiO$_x$ films produced from sputtering, solgel or nanocrystal routes and their CV behavior. (a) Depiction of NiO$_x$ surface structure and species. (b) Photos of various NiO$_x$ film precursors and corresponding SEM images (scale bar: 500 nm). (c) Progressive CV on film formed from NiO$_x$ nanoparticles. OER: oxygen evolution region. (d) CV scan comparing the different types of NiO$_x$ showing obvious variations in the redox behavior.

shrink and grow surface phases resulting in gradual breakdown of the cubic NiO structure as observed for the instability of electrochromic devices.[36–38] The plausibility of alternative phases and surface species on a purely cubic NiO crystal is depicted in Fig. 1a.

Thin films of NiO$_x$ can be processed in a variety of ways for PSCs such as sputtered, solgel, and nanoparticle NiO$_x$ routes shown in Fig. 1b, which also shows differences in appearance of the starting materials and resulting morphology visible by SEM. Visually, the source material colors vary between green, gray and black, where sputtered forms appear light gray/green, sol–gel NiO$_x$ precursor are more vibrant green, and nanoparticles are often black. Color variations are mainly due to non-stoichiometry, defects (vacancies or various oxidation states like Ni^{3+}), and quantum size effects.[39–41]

NiO$_x$ aqueous electrochemistry

Electrochemical properties, reactions, and phase changes in aqueous electrolytes are widely studied for NiO$_x$s.[23,37,38,42] Notably, NiO$_x$ rarely behaves as an ideal semiconductor (transfers valence band holes to the redox couple) when driving redox reactions. Instead, it often behaves as an electrocatalyst where near surface and surface Ni changes oxidation states between 0

and 4+.[23,38,43–45] Regarding the oxygen evolution reaction (OER), it is known the highly oxidizing Ni^{4+} state reacts with adsorbed water to form peroxides, which then subsequently react to release O$_2$ in a catalytic fashion.[23]

Fig. 1c shows progressive CV scans on NiO$_x$ films from nanoparticles with different intervals starting from −0.1 V *versus* Ag|AgCl (1 M) to 0.5–1.1 V, increasing the anodic range by 0.1 V every 3 cycles, in 0.5 M KCl at natural pH (∼5.5). A bare tin-doped indium oxide (ITO) control is also plotted for comparison. The ITO control shows a nearly square CV, which is just the double layer capacitance. The NiO$_x$ shows much higher current density, which we attribute to redox activity of the NiO$_x$ surface. Notably, we observe three distinguishable regions. The low potential feature (∼0.2 V) only appears and grows when the anodic voltage exceeds 0.6 V, and we attribute this to an adsorbed species formed by reacting with electrochemically induced Ni^{3+}. This feature is plausibly a peroxide or other reactive oxygen species that forms at specific reactive surface sites. We verified that our measurement does not involve K intercalation reactions by an independent measurement in hexyltrimethylammonium bromide (Fig. S1) where such a bulky cation cannot intercalate into a layered NiO$_x$ structure. We hypothesize that these surface adsorption/reaction sites should

be eliminated or blocked for optimal PSC performance. Chemical reactions can release detrimental defects and impurities during device fabrication and operation.

Between 0.4–0.8 V corresponds primarily to $Ni^{2+/3+}$ transitions (and is also the electrochromic transition region) such as β-$Ni(OH)_2$ → β-NiOOH.[37,38,46] Beyond 0.8 V, higher oxidation states are possible in phases like γ-NiOOH and eventually Ni^{4+} can induce OER.[23,37] Moreover, while the characteristics vary, we observe the same general features irrespective of the NiO_x processing route as shown in Fig. 1d, yet the PSC performance on these different NiO_xs also vary widely (Fig. S2). Sol–gel NiO_x and as-deposited (room temperature) sputtered NiO_xs often display large redox activity, which is significantly decreased with increasing annealing temperature (Fig. S3).

Frequently, despite having a high surface area, we observe nanoparticle NiO_x to have the lowest CV current density, irrespective of annealing temperature, and most distinct features which may be a result of calcination at high temperatures during synthesis. This step should facilitate the lowest impurity phase content (cubic NiO_x conversion occurs $>350\ ^\circ C$[47,48]), highest crystallinity, and a simple process that does not drift over time, providing excellent reproducibility (Fig. S4). Our early exploration using electrochemical characterization revealed our NiO_x sputtering process drifted over the course of several months depending on the age of the target or contamination from other oxide targets in the system. Additionally, sol–gel NiO_x electrochemical features were strongly dependent on the annealing temperature and ambient conditions. For this reason, we focus on this nanoparticle NiO_x as a model system throughout this study to characterize further and fabricate PSCs. This allowed us to repeat the quantifications and statistical analyses discussed in the following sections several times to improve our confidence in the results.

Our electrochemical measurement selectively probes the redox active species at an electrode surface which is what we specifically target in this work. It should be sensitive to subtle changes to the surface termination, dopants, and ligands on various NiO_x materials. Moreover, it induces changes to or formation of reactive species in response to anodic potentials that the NiO_x anodes experience *in operando* in PSCs. It is important to note that we believe KCl aqueous electrochemistry

at pH < 7 is a suitable proxy for the redox activity of NiO_x when in contact with halide perovskite solutions and solids. Both environments are highly polar, protic (from labile H^+ on MA and FA), and contain halides. Additionally, in the perovskite system, methylamine and NH_3 originating from cation degradation may coordinate to ions or surfaces similarly as H_2O.

The surface properties of the NiO_x particles were also characterized by Fourier transform infrared spectroscopy (FTIR) and X-ray photoemission spectroscopy (XPS). FTIR showed a distinct change in the OH content of the NiO_x sample (Fig. S5). The Ni $2p_{3/2}$ spectrum of the bare NiO_x particles control (Fig. S6) indeed deviates from that of a NiO reference. The intensity variation at the higher binding energy region (indicated by an arrow) of the main line peak is attributed to the presence of a variety of Ni–OH species, including α-$Ni(OH)_2$, β-$Ni(OH)_2$, β-NiOOH, and γ-NiOOH, agreeing with the CV measurements. Note, however, that XPS is not able to distinguish between these Ni–OH species,[49] so as a representative spectrum, only γ-NiOOH is shown in Fig. S6. The sample environments during measurements differ, with the likelihood of the formation of Ni–OH species being significantly higher in the aqueous environment of CV than the UHV of XPS. Nevertheless, the measurements in UHV are still in agreement with an average Ni oxidation state $>2+$. This is predictive of the increased redox active states, as discussed above.

CV to observe and quantify passivation

NiO_x is often used in combination with an organic layer or surface modifier to improved PSC efficiency where a common passivation treatment is to apply PACzs.[50–54] This can be viewed as a ligand exchange which is common while processing nanoparticles into functional films.[55] From our FTIR, the main ligand observed was OH (Fig. S5). However, changes to the reactive sites on NiO_x surfaces by PACz passivation have not yet been investigated in detail, and we will show optimal passivation is somewhat more complicated than a ligand exchange.

Fig. 2a shows electrochemical CV results for NiO_x and NiO_x treated with (4-(3,6-dimethyl-9*H*-carbazol-9-yl)butyl)phosphonic acid (Me-4PACz). The measurement reveals that the overall curve for NiO_x/Me-4PACz is narrower compared to the NiO_x control. The region where the control develops a new absorbed
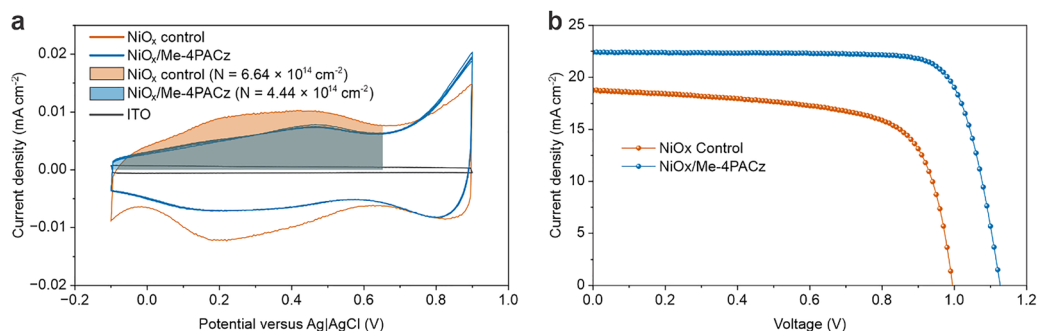

Fig. 2 CV and JV comparison between passivated and un-passivated NiO_x. (a) CV for nanoparticle NiO_x and NiO_x/Me-4PACz. (b) JV for NiO_x based PSC and NiO_x/Me-4PACz based PSCs.

species forms during the CV is drastically suppressed, while the $Ni^{2+/3+}$ electrochromic region is slightly suppressed (shaded regions under the curves). The features in the CV of NiO_x indicate that the NiO_x surface is electrochemically active, and we hypothesize that attaching a molecule to that surface site could substantially reduce the electrochemical activity of NiO_x have a positive effect on solar cell metrics. We fabricated PSCs using the NiO_x and NiO_x/Me-4PACz (device architecture and processing details in methods) where the Me-4PACz passivation dramatically improves the PCE. This directly supports our hypothesis and correlation to electrochemical CV properties. Moreover, this effect is general to all types of NiO_x (Fig. S7).

The shaded region in Fig. 2a is integrated (subtracting the ITO double layer capacitance value) to derive the charge passed during this section of the CV (units cm^{-2}) which we call N. The calculation of N is described by eqn (1):

$$N = \frac{\Delta V}{e\nu} \sum_{0.65}^{-0.1} J(V) \tag{1}$$

where ΔV is the voltage step size, e is the electron charge, ν is the scan rate, and J is the measured current density. This quantity represents the surface redox activity of NiO_x. The Cz groups are sometimes oxidized (i.e. $Cz^0 \rightarrow Cz^+$) at potentials > 0.65 V as shown by ITO/PACz controls. The chosen voltage window isolates the redox processes associated with NiO_x, as the oxidation of Me-4PACz would otherwise skew the assessment of intrinsic NiO_x redox behavior (Fig. S8).

NiO_x surface passivation in perovskite solar cells

We applied this analytic electrochemical method capable of quantifying the density of electrochemically active sites on the NiO_x surface for a set of PACz molecules with various lengths and side groups shown in Fig. 3a. The 3,6 position side groups on the Cz molecule modify their energy levels by their electron donating or withdrawing nature. To assess the influence of these PACzs on device performance, we fabricated PSCs with an inverted (p–i–n) structure of Glass/ITO/nanoparticle NiO_x/PACz/ Perovskite/Phenethylammonium chloride (PEACl)/Phenyl C61 butyric acid methyl ester (PC$_{61}$BM)/ALD-SnO$_x$/Ag (Fig. 3b). Note, we had no complications from coating wettability of the perovskite ink which is a well-known problem when the SAMs are full coverage.[56] Therefore, our SAMs are most likely *not* full coverage, their primary impact is defect passivation of the NiO_x, and the NiO_x remains capable of functioning as the primary hole extracting material. The N-value obtained from the CVs (Fig. S9) for the NiO_x/PACzs in Fig. 3c shows that the effectiveness of decreasing the redox activity of the NiO_x surface varies by a factor of 4–5 (ΔN versus the NiO_x control, order of magnitude $\sim 10^{14}$ cm^{-2}). The PSC device parameters PCE, open-circuit voltage (V_{OC}), fill factor (FF), and short-circuit current density (J_{SC}) from J–V measurements under AM1.5G simulated solar illumination are shown in Fig. 3d.

We plot the device parameters versus N in Fig. 3e which exhibits a negative correlation between N and all major photovoltaic performance metrics. This relationship is further confirmed by calculating the double-sided P-values using the Pearson's R coefficient and the degrees of freedom to be ≤ 0.012. This indicates that the N-value is correlated to device metrics with > 98.8% confidence, and the probability of the null hypothesis that the correlation is due to random chance is < 1.2%. The P-values for J_{SC}, FF, and PCE are lower than for V_{OC}, which allows us to be even more confident in the statistical significance of the N-value correlations for these metrics. From these plots, a clear correlation emerges between the redox activity of the NiO_x/SAM interface and key photovoltaic parameters. Devices incorporating SAMs that exhibit higher interfacial redox activity tend to show inferior efficiency. Overall, the device PCE is influenced by many factors such as subtle differences in perovskite crystallization, but the correlation analysis shows that increased electrochemical activity at the interface detrimentally affects the electronic quality of the device.

Notably, all metrics V_{OC}, J_{SC}, and FF, and therefore PCE, are improved in devices employing PACzs compared to unpassivated NiO_x-based controls as depicted in Fig. 3d. This enhancement is further supported by the observed decrease in the integrated current observed in CV measurements, indicating more efficient charge carrier transport and reduced interfacial trap density. These device improvements are similarly reflected in optoelectronic property characterization where the same trend is observed in quasi-Fermi level splitting (QFLS) measurements derived from photoluminescence quantum yield (PLQY) and photocarrier lifetime (a negative correlation between QFLS and N, Fig. S10). This suggests the reactive surface sites contribute to unwanted non-radiative recombination in our devices.

Among the PA carbazoles studied, Me-4PACz yields the lowest N-value (4.44×10^{14} cm^{-2}) and simultaneously delivers the highest average device efficiency, indicating superior passivation capability. MeO-2PACz appears as an outlier in the N-value correlation plot compared to other PA carbazoles derivatives. This is attributed to pronounced redox features observed near 0.1 V and 0.6 V (Fig. S8c), which contribute to the elevated N. This excess current density is likely a property of MeO-2PACz and not the underlying NiO_x. For this reason, we regard MeO-2PACz N as an outlier, and do not include it in the statistical correlation analyses. We see similar extra reactivity for MeO-4PACz on ITO, but the NiO_x/MeO-4PACz has no obvious excessive current density in early cycles allowing us to quantify the reduction in N and include it in the statistical analyses.

Mechanism investigation

In our previous study, we demonstrated that higher Ni oxidation states on NiO_x surfaces will oxidize iodide, but only in the presence of certain additional reactants.[7] Briefly, MAI and FAI will react, while PbI$_2$, CsI, MABr, and FABr will not. This confirms that a protic Brønsted acid is needed to react along with the reducing agent (iodide in this case). The reaction for halide perovskite salts with high oxidation state Ni surface species (e.g. Ni^{3+}) is given by eqn (2) adapted from Boyd, C. C.
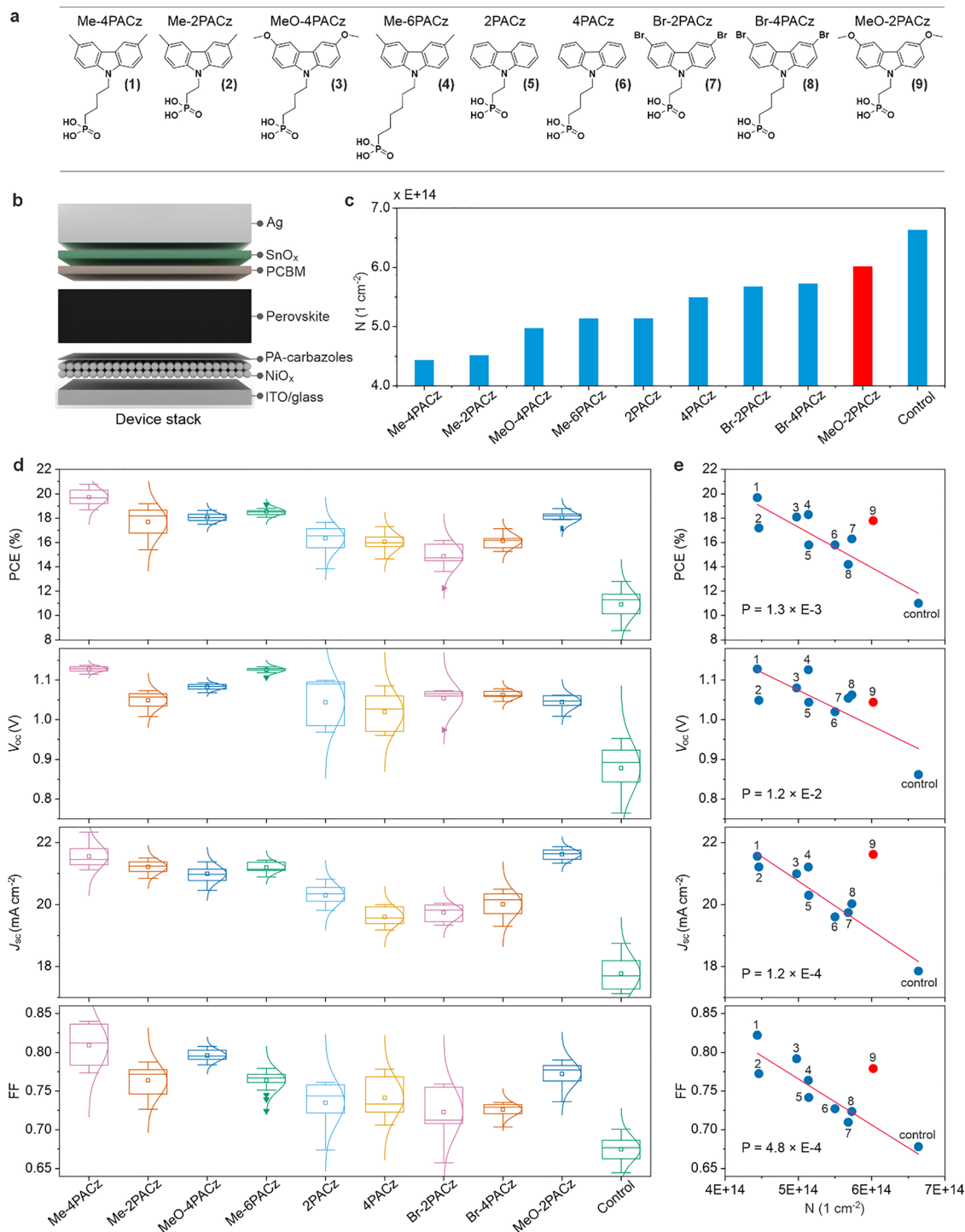
Fig. 3 PA carbazole passivation effects and their correlation to N-value. (a) Molecular structure of PA carbazoles. (b) Device structure. (c) N-value for various PA carbazoles on NiO_x. (d) Perovskite solar cell performance based on NiO_x passivated with different PA carbazoles. (e) Correlation between N-value and perovskite solar cell performance.

et al.[7] which is a proton transfer-electron transfer reaction:

$$HAPbI_3 + Ni^{\geq 3+}O_x \rightarrow PbI_2 + \frac{1}{2}I_2 + A + Ni^{\geq 2+}O_xH \quad (2)$$
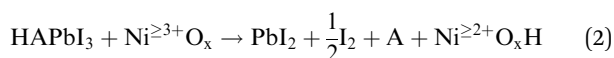
In the case of PACzs, the PA is naturally the Brønsted acid. Most of the acid groups likely react with NiOH and NiO surface species *via* a straightforward acid–base reaction resulting in a variety of bidentate and tridentate attachments. Such an acid–base reaction does not necessarily discriminate between Ni^{2+} and Ni^{3+} but cannot change their oxidation states. We are left to assume the most problematic Ni^{3+} sites are eliminated by Cz acting as the reducing agent despite its deep highest occupied

This journal is © The Royal Society of Chemistry 2026
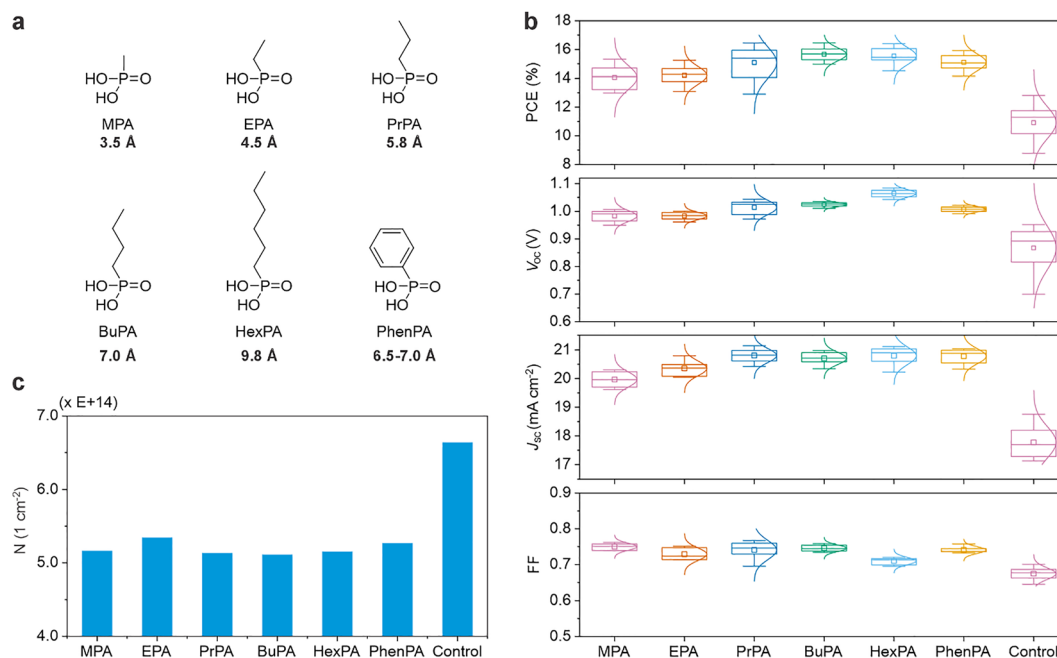
Energy Environ. Sci., 2026, **19**, 884–895 | **889**

Fig. 4 Alkyl-PAs passivation effects and their correlation to N-value. (a) Molecular structure of various alkyl-PAs. (b) Perovskite solar cell performance based on NiO$_x$ passivated with different alkyl-PAs (c) N-values corresponding to different alkyl-PAs on NiO$_x$.

molecular orbital (HOMO, also known as the ionization potential). Following eqn (2), a reaction specific to passivating high oxidation state Ni is shown in eqn (3) where $n = 2$ or 4 for the alkyl chain.

$$Cz^0(CH_2)_nPO(OH)_2 + Ni^{3+}O^{2-} \rightarrow$$
$$Cz^+(CH_2)_n[PO_2OH]^- + Ni^{2+}(OH)^- \quad (3)$$
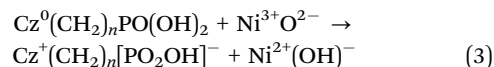
Note the importance of having both the Cz reducing agent and acidic PA to transfer a proton for the passivation reaction, which is distinct from the mere PA/OH surface attachment reaction. To test the above hypotheses, we performed CV on NiO$_x$ treated with phosphoric acid and hypophosphorous acid (Fig. S11) which showed no passivation by phosphoric acid, and some for hypophosphorous acid. Hypophosphorous acid is a reducing agent, consistent with the mechanisms proposed above.

Thus, we applied the same methodology, treating the NiO$_x$ with alkyl PAs with systematically varied alkyl chain lengths from methylphosphonic acid to hexylphosphonic acid as shown in Fig. 4a, to explore the relationship between molecular length, possible differences in surface packing, physically spacing the perovskite from the NiO$_x$ on the overall device performance. The CV-derived N-values (Fig. S12) for these molecules are shown in Fig. 4b which are all essentially equivalent. While some passivation is observed, none of these simple molecules minimize the redox activity as effectively as Me-4PACz despite being able to pack more densely than PACzs. As shown in Fig. 4c, all the alkyl-PAs examined contribute to slightly improved device efficiency relative to un-passivated NiO$_x$, demonstrating effective passivation behavior even at the

expense of an obvious charge extraction barrier (*e.g.* lowered FF for HexPA).

These performance variations align with the redox activity of the alkyl-PAs-treated NiO$_x$, as quantified by the integrated N-value from CV measurements, shown in Fig. S12. Bare NiO$_x$ exhibited a high N-value of 6.64×10^{14} cm^{-2}, correlating with moderate PCE values ranging from 9% to 12% and V_{OC} values between 0.90 and 0.95 V. Upon passivation with alkyl-PAs, the N-value decreased to ~ 5.11–5.30×10^{14} cm^{-2}, indicating suppressed redox activity and chemical reactivity, which corresponded with enhanced PCE, V_{OC}, J_{SC}, and FF compared to unpassivated controls. There was no clear trend in the tail length on N, but increasing tail length appears to slightly improve device metrics. Because the alkyl PAs all had essentially the same N-value, a correlation could not be extracted for this experiment alone. However, we aggregated the device metric *versus* N-value for all the SAMs in this study in Fig. S13. This analysis shows that the overall negative correlation trendline between N-values and device efficiency is strengthened by including the alkyl-PA data, reducing the probability that the null hypothesis (no correlation between N-value and device metrics) is true to $<0.4\%$. This confirms that effective suppression of NiO$_x$ surface redox reactions is a key determinant of improved photovoltaic performance when nonradiative recombination is limiting.

All the alkyl PAs lacking a reducing agent were unable to obtain the level of passivation realized by Me-4PACz, Me-2PACz, and MeO-4PACz (and, presumably MeO-2PACz). Additionally, Cz alone (no acidic protons) did not show any passivation *via* CV (Fig. S14). Thus, the data is consistent with the hypothesis that full passivation of the variety of reactive surface sites requires both a reducing agent and Brønsted acid.
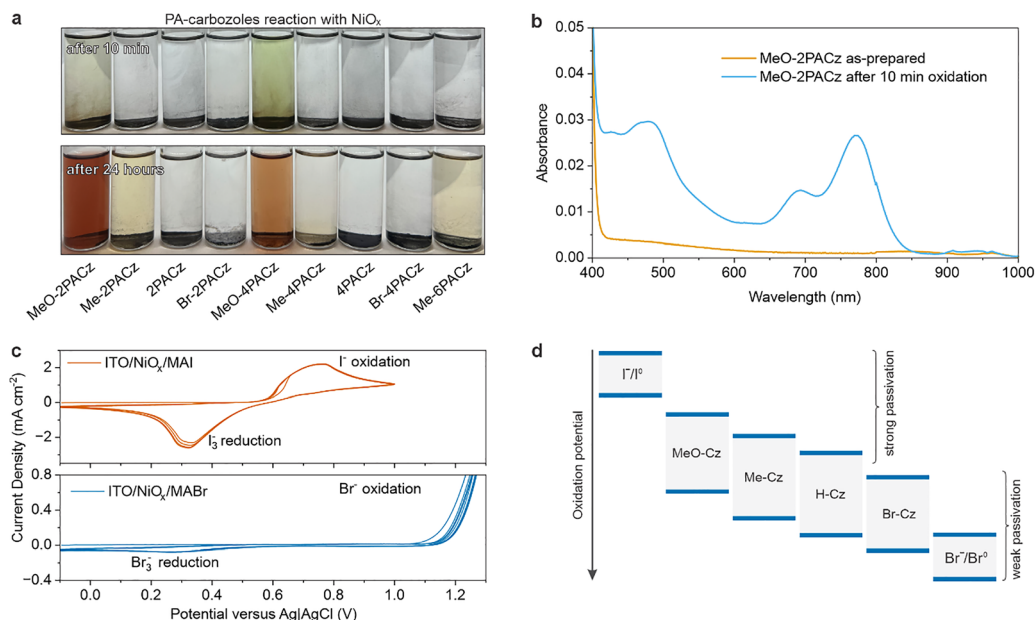
890 | *Energy Environ. Sci.*, 2026, **19**, 884–895

This journal is © The Royal Society of Chemistry 2026

Fig. 5 PA carbazoles reaction and energy level comparison. (a) PACz reaction with "NiO$_2$" after 10 min and after 24 h. (b) UV-vis data for MeO-2PACz in ethanol/water before and after reaction with "NiO$_2$" ($\sim$20–30 min). (c) CV of NiO$_x$ films in the presence of $\sim$10 mM MAI and MABr (0.5 M KCl supporting electrolyte). (d) Relative oxidation potential for PA carbazoles, I$^-$/I^0, Br$^-$/Br^0 derived from the CV measurements.

To examine this hypothesis further, we tested if Ni^{3+} or Ni^{4+} can lead to sufficiently oxidizing conditions to oxidize these Czs. In this experiment, we dissolved PACzs in ethanol and added to a mixture of commercially advertised NiO$_2$ particles in water. Notably, upon mixing NiO$_2$ powder with PACz solutions where the Cz units contain electron-donating methoxy substituents—specifically MeO-2PACz and MeO-4PACz—the solutions exhibited an immediate color change to green (Fig. 5a), indicative of radical cation formation.[57] Aliquots of the MeO-2PACz before and after (filtered to remove trace NiO$_x$) interaction with NiO$_2$ was characterized by UV-visible spectroscopy. As illustrated in Fig. 5b, new absorption features emerged around 760 nm and 400 nm following exposure, which are consistent with the spectroscopic fingerprints of oxidized carbazoles.[58,59]

Over the course of approximately 70 minutes, the MeO-PACz solutions transitioned to an orange hue, suggesting the progression of further chemical reactions (Fig. S15). Me-2-, Me-4-, and Me-6PACz displayed a slower response, with a visible color change emerging only after prolonged exposure (approximately one day) to NiO$_2$ powder, as shown in Fig. 5a. These observations support the hypothesis that the more highly passivating PACzs can be oxidized in the presence of NiO$_x$ with Ni^{4+}, Ni^{3+}, or the species that adsorb to these sites (e.g. peroxides).

The observed reactivity also follows the expected trend for the Cz HOMO energies given the electron donating/withdrawing strength of the side groups. The HOMO energy is related to the oxidation potential of a molecule.[60] One would anticipate the |HOMO| series to follow MeO < Me < H < Br. CV in the KCl only electrolyte on ITO/PACz samples, where the Cz is the main species participating in electrochemical redox, provides direct confirmation of this trend where we extrapolated the

relative oxidation potentials in Fig. S16. Furthermore, we measured the oxidation potentials of iodide and bromide ($\sim$10 mM in the 0.5 M KCl supporting electrolyte) at the ITO/NiO$_x$ interface (Fig. 5c). These data are fully consistent with our previous observation on the lack of reactivity for MABr and FABr[7] because bromide is too difficult to oxidize, while iodide is easier to oxidize than Cz groups. We then compiled all these measured relative oxidation potentials in Fig. 5d. PACzs bearing MeO groups at the 3,6-positions exhibit the shallowest HOMO energy levels, rendering them more capable of reducing Ni^{3+} reactive sites. In contrast, SAMs with electron-withdrawing groups, such as bromo-substituted carbazole derivatives, possess deeper HOMO levels and are thus less capable of reducing Ni^{3+}. As a consequence, deeper HOMO SAMs are less effective at suppressing the redox activity of NiO$_x$ surfaces, leading to increased interfacial recombination/degradation and diminished device performance, fully consistent with our N-value analyses.

This phenomenon reveals that PACzs, and passivation agent combinations more generally, play multiple roles in NiO$_x$-based perovskite solar cells. First, the PA group passivates some surface sites on its own via acid–base reactions. Second, the Cz moiety with HOMO equivalent to Me-PACzs or shallower (≤ 5.4 eV, approximately) reduces Ni^{3+} defects by transferring electrons from the HOMO to Ni^{3+} involving additional proton transfer. The combination of these properties provides the fullest passivation. Note, a precise HOMO energy/oxidation potential is difficult to accurately measure and highly dependent on many properties, including how the reducing agent coordinates to the Ni^{3+}. Thus, it is difficult to predict the subtle differences in passivation. Much more work on this topic is necessary. Third, there is also the effect of physical buffering

the perovskite from the NiO_x surface, such as length and coverage of PAs or PACzs. The full combination of mechanisms helps suppress detrimental oxidative interactions, such as the oxidation of iodide (I^-) to molecular iodine (I_2) and MA and FA degradation in the perovskite layer, thereby enhancing PSC efficiency.

Wider implications

Our results on NiO_x/PACz passivation are consistent with several recent reports of high PCE PSCs as well as a study on OPVs. Peng et al. observed improvements to PSC performance in the order Me-4PACz > 2PACz > Br-4PACz.[61] Angus et al. observed NiO_x/Me-4PACz to significantly outperform NiO_x/2PACz for two different perovskite compositions, consistent with our observation that 2PACz provides only slight passivation for NiO_x.[62] Their MeO-2PACz was much more variable, which may align with the complex reactivity of this molecule we observed. Finally, a recent OPV study combining NiO_x and SAMs observed PCE order ((4-(7H-dibenzo[c,g]carbazol-7-yl)butyl)phosphonic acid (CbzNaph) > 2PACz > Br-2PACz.[9] The CbzNaph has a shallower HOMO than 2PACz.[63] These observations fit our trend of shallower HOMO PACzs more effectively passivating NiO_x. Thus, the impact of the reactivity of NiO_x, our fundamental insight on the relationship to HOMO and passivation, and our method for quantifying these redox active surface site densities may be broadly applicable to optoelectronic devices. The electrochemical data can be combined with information such as energy level alignments and interfacial conductivity for a more comprehensive understanding of device performance.

Overall, the results indicate that mixtures of acids and reducing agents should be explored as passivation agents and surface modifiers for NiO_x hole extraction layers. Reducing agents with oxidation potentials ≤ 5.4 eV (with respect to vacuum) are most promising, but the influence of pK_a of the acid groups requires more exploration. Performing our CV protocol will provide additional insight. The surface treatment parameter space is obviously extremely large, but our CV method can be used to screen many conditions and mixtures of promising candidates without having to make a full solar cell. This measurement could also be easily adapted to quality control and process variability characterization contributing to commercialization efforts in other ways.

Conclusion

In summary, we present a systematic study of surface passivation of NiO_x-based hole transport layers in perovskite solar cells using PACz molecules to bind to, react with, and occupy detrimental surface states that can limit solar cell efficiency through non-radiative recombination. We demonstrate a novel electrochemical characterization and proxy quantification of the surface density of reactive sites and make statistically significant correlations to PSC device efficiency. Our

introduction of the N-value—a quantitative electrochemical descriptor of NiO_x reactivity—enables direct correlation between surface passivation efficacy and device performance. Finally, we identify the key roles of interface reactivity and proton availability in modulating surface redox behavior of NiO_x. This study provides mechanistic insights and practical guidelines for the rational design of next-generation materials for PSCs and other devices underscoring the critical importance of interface engineering in metal halide perovskite technologies.

Author contributions

Conflicts of interest

There are no conflicts to declare.

Data availability

The data supporting the findings of this study are available within the article and its supplementary information (SI). Additional raw data is available upon reasonable request. Supplementary information is available. See DOI: https://doi.org/10.1039/d5ee05065k.

Acknowledgements

892 | Energy Environ. Sci., 2026, 19, 884–895

This journal is © The Royal Society of Chemistry 2026

References

1 J. Lin, X. Dai, X. Liang, D. Chen, X. Zheng and Y. Li, *et al.*, High-Performance Quantum-Dot Light-Emitting Diodes Using NiOx Hole-Injection Layers with a High and Stable Work Function, *Adv. Funct. Mater.*, 2020, **30**(5), 1907265, DOI: 10.1002/adfm.201907265.

2 R. Islam, G. Chen, P. Ramesh, J. Suh, N. Fuchigami and D. Lee, *et al.*, Investigation of the Changes in Electronic Properties of Nickel Oxide (NiOx) Due to UV/Ozone Treatment, *ACS Appl. Mater. Interfaces*, 2017, **9**(20), 17201–17207, DOI: 10.1021/acsami.7b01629.

3 E. L. Ratcliff, J. Meyer, K. X. Steirer, A. Garcia, J. J. Berry and D. S. Ginley, *et al.*, Evidence for near-Surface NiOOH Species in Solution-Processed NiOx Selective Interlayer Materials: Impact on Energetics and the Performance of Polymer Bulk Heterojunction Photovoltaics, *Chem. Mater.*, 2011, **23**(22), 4988–5000, DOI: 10.1021/cm202296p.

4 M. D. Irwin, D. B. Buchholz, A. W. Hains, R. P. H. Chang and T. J. Marks, p-Type semiconducting nickel oxide as an efficiency-enhancing anode interfacial layer in polymer bulk-heterojunction solar cells, *Proc. Natl. Acad. Sci. U. S. A.*, 2008, **105**(8), 2783–2787, DOI: 10.1073/pnas.0711990105.

5 K. X. Steirer, P. F. Ndione, N. E. Widjonarko, M. T. Lloyd, J. Meyer and E. L. Ratcliff, *et al.*, Enhanced Efficiency in Plastic Solar Cells via Energy Matched Solution Processed NiOx Interlayers, *Adv. Energy Mater.*, 2011, **1**(5), 813–820, DOI: 10.1002/aenm.201100234.

6 B. Li, C. Zhang, D. Gao, X. Sun, S. Zhang and Z. Li, *et al.*, Suppressing Oxidation at Perovskite–NiOx Interface for Efficient and Stable Tin Perovskite Solar Cells, *Adv. Mater.*, 2024, **36**(17), 2309768, DOI: 10.1002/adma.202309768.

7 C. C. Boyd, R. C. Shallcross, T. Moot, R. Kerner, L. Bertoluzzi and A. Onno, *et al.*, Overcoming Redox Reactions at Perovskite-Nickel Oxide Interfaces to Boost Voltages in Perovskite Solar Cells, *Joule*, 2020, **4**(8), 1759–1775. Available from: https://www.sciencedirect.com/science/article/pii/S2542435120302415.

8 G. Li, Y. Jiang, S. Deng, A. Tam, P. Xu and M. Wong, *et al.*, Overcoming the Limitations of Sputtered Nickel Oxide for High-Efficiency and Large-Area Perovskite Solar Cells, *Adv. Sci.*, 2017, **4**(12), 1700463, DOI: 10.1002/advs.201700463.

9 D. Garcia Romero, G. Bontekoe, J. Pinna, L. Di Mario, C. M. Ibarra-Barreno and J. Kardula, *et al.*, 80% Fill Factor in Organic Solar Cells with a Modified Nickel Oxide Interlayer, *Adv. Energy Mater.*, 2025, 2404981, DOI: 10.1002/aenm.202404981.

10 B. B. O. Seibertz and B. Szyszka, P-type nickel oxide deposited by reactive hollow cathode gas flow sputtering for the potential usage in thin-film transistors, *Thin Solid Films*, 2023, **778**, 139887.

11 H. Wan, E. D. Jung, T. Zhu, S. M. Park, J. M. Pina and P. Xia, *et al.*, Nickel Oxide Hole Injection Layers for Balanced Charge Injection in Quantum Dot Light-Emitting Diodes, *Small*, 2024, **20**(34), 2402371, DOI: 10.1002/smll.202402371.

12 J. R. Castillo-Saenz, N. Nedev, B. Valdez-Salas, M. Bernechea, E. Martínez-Guerra and I. Mendivil-Palma, *et al.*, Effect of oxidation temperature on the properties of NiOx layers for application in optical sensors, *Thin Solid Films*, 2021, **734**, 138849. Available from: https://www.sciencedirect.com/science/article/pii/S0040609021003321.

13 T. P. Mokoena, H. C. Swart and D. E. Motaung, A review on recent progress of p-type nickel oxide based gas sensors: Future perspectives, *J. Alloys Compd.*, 2019, **805**, 267–294. Available from: https://www.sciencedirect.com/science/article/pii/S092583881932420X.

14 C. Li, X. Wang, E. Bi, F. Jiang, S. M. Park and Y. Li, *et al.*, Rational design of Lewis base molecules for stable and efficient inverted perovskite solar cells, *Science*, 2023, **379**(6633), 690–694, DOI: 10.1126/science.ade3970.

15 A. E. Louks, R. Tirawat, M. Yang, S. N. Habisreutinger, S. P. Harvey and K. Schutt, *et al.*, Improving Stability of Triple-Cation Perovskite Solar Cells under High-Temperature Operation, *Sol. RRL*, 2023, **7**(16), 2300248, DOI: 10.1002/solr.202300248.

16 J. Xia, Y. Zhang, C. Xiao, K. G. Brooks, M. Chen and J. Luo, *et al.*, Tailoring electric dipole of hole-transporting material p-dopants for perovskite solar cells, *Joule*, 2022, **6**(7), 1689–1709, DOI: 10.1016/j.joule.2022.05.012.

17 T. H. Schloemer, T. S. Gehan, J. A. Christians, D. G. Mitchell, A. Dixon and Z. Li, *et al.*, Thermally Stable Perovskite Solar Cells by Systematic Molecular Design of the Hole-Transport Layer, *ACS Energy Lett.*, 2019, **4**(2), 473–482, DOI: 10.1021/acsenergylett.8b02431.

18 S. Ahmad, R. Ma, J. Zheng, C. K. Gary Kwok, Q. Zhou and Z. Ren, *et al.*, Suppressing Nickel Oxide/Perovskite Interface Redox Reaction and Defects for Highly Performed and Stable Inverted Perovskite Solar Cells, *Small Methods*, 2022, **6**(10), 2200787, DOI: 10.1002/smtd.202200787.

19 T. Wu, L. K. Ono, R. Yoshioka, C. Ding, C. Zhang and S. Mariotti, *et al.*, Elimination of light-induced degradation at the nickel oxide-perovskite heterojunction by aprotic sulfonium layers towards long-term operationally stable inverted perovskite solar cells, *Energy Environ. Sci.*, 2022, **15**(11), 4612–4624, DOI: 10.1039/D2EE01801B.

20 S. Thampy, B. Zhang, K.-H. Hong, K. Cho and J. W. P. Hsu, Altered Stability and Degradation Pathway of CH3NH3PbI3

in Contact with Metal Oxide, *ACS Energy Lett.*, 2020, **5**(4), 1147–1152, DOI: 10.1021/acsenergylett.0c00041.

21 W. A. Dunlap-Shohl, T. Li and D. B. Mitzi, Interfacial Effects during Rapid Lamination within MAPbI3 Thin Films and Solar Cells, *ACS Appl. Energy Mater.*, 2019, **2**(7), 5083–5093, DOI: 10.1021/acsaem.9b00747.

22 D. Sharma, R. Mehra and B. Raj, Comparative study of hole transporting layers commonly used in high-efficiency perovskite solar cells, *J. Mater. Sci.*, 2022, **57**(45), 21172–21191, DOI: 10.1007/s10853-022-07958-3.

23 K. Juodkazis, J. Juodkazytė, R. Vilkauskaitė and V. Jasulaitienė, Nickel surface anodic oxidation and electrocatalysis of oxygen evolution, *J. Solid State Electrochem.*, 2008, **12**(11), 1469–1479, DOI: 10.1007/s10008-007-0484-0.

24 R. Blume, W. Calvet, A. Ghafari, T. Mayer, A. Knop-Gericke and R. Schlögl, Structural and Chemical Properties of NiOx Thin Films: Oxygen Vacancy Formation in O2 Atmosphere, *ChemPhysChem*, 2023, **24**(23), e202300231, DOI: 10.1002/cphc.202300231.

25 B. Li, C. Zhang, D. Gao, X. Sun, S. Zhang and Z. Li, *et al.*, Suppressing Oxidation at Perovskite–NiO Interface for Efficient and Stable Tin Perovskite Solar Cells, *Adv. Mater.*, 2024, **36**(17), 2309768, DOI: 10.1002/adma.202309768.

26 A. Swarnkar, A. R. Marshall, E. M. Sanehira, B. D. Chernomordik, D. T. Moore and J. A. Christians, *et al.*, Quantum dot–induced phase stabilization of α-CsPbI3 perovskite for high-efficiency photovoltaics, *Science*, 2016, **354**(6308), 92–95, DOI: 10.1126/science.aag2700.

27 Y. Yang, S. Cheng, X. Zhu, S. Li, Z. Zheng and K. Zhao, *et al.*, Inverted perovskite solar cells with over 2000 h operational stability at 85 °C using fixed charge passivation, *Nat. Energy*, 2024, **9**(1), 37–46, DOI: 10.1038/s41560-023-01377-7.

28 M. Bonomo, D. Dini and A. G. Marrani, Adsorption Behavior of I3– and I– Ions at a Nanoporous NiO/Acetonitrile Interface Studied by X-ray Photoelectron Spectroscopy, *Langmuir*, 2016, **32**(44), 11540–11550, DOI: 10.1021/acs.langmuir.6b03695.

29 Y.-F. Li, J.-L. Li and Z.-P. Liu, Structure and Catalysis of NiOOH: Recent Advances on Atomic Simulation, *J. Phys. Chem. C*, 2021, **125**(49), 27033–27045, DOI: 10.1021/acs.jpcc.1c06170.

30 E. A. Gibson, M. Awais, D. Dini, D. P. Dowling, M. T. Pryce and J. G. Vos, *et al.*, Dye sensitised solar cells with nickel oxide photocathodes prepared via scalable microwave sintering, *Phys. Chem. Chem. Phys.*, 2013, **15**(7), 2411–2420, DOI: 10.1039/C2CP43592F.

31 T. P. Murphy and M. G. Hutchins, Oxidation states in nickel oxide electrochromism, *Sol. Energy Mater. Solar Cells*, 1995, **39**(2), 377–389. Available from: https://www.sciencedirect.com/science/article/pii/0927024896800031.

32 K. X. Steirer, R. E. Richards, A. K. Sigdel, A. Garcia, P. F. Ndione and S. Hammond, *et al.*, Nickel oxide interlayer films from nickel formate–ethylenediamine precursor: influence of annealing on thin film properties and photovoltaic device performance, *J. Mater. Chem. A*, 2015, **3**(20), 10949–10958, DOI: 10.1039/C5TA01379H.

33 S. Dey, S. Bhattacharjee, M. G. Chaudhuri, R. S. Bose, S. Halder and C. K. Ghosh, Synthesis of pure nickel(iii) oxide nanoparticles at room temperature for Cr(vi) ion removal, *RSC Adv.*, 2015, **5**(67), 54717–54726, DOI: 10.1039/C5RA05810D.

34 M. Fingerle, S. Tengeler, W. Calvet, W. Jaegermann and T. Mayer, Sputtered Nickel Oxide Thin Films on n-Si(100)/SiO2 Surfaces for Photo-Electrochemical Oxygen Evolution Reaction (OER): Impact of Deposition Temperature on OER Performance and on Composition before and after OER, *J. Electrochem. Soc.*, 2020, **167**(13), 136514, DOI: 10.1149/1945-7111/abbcdf.

35 J. Zhang, J. R. Winkler, H. B. Gray and B. M. Hunter, Mechanism of Nickel–Iron Water Oxidation Electrocatalysts, *Energy Fuels*, 2021, **35**(23), 19164–19169, DOI: 10.1021/acs.energyfuels.1c02674.

36 M. Z. Sialvi, R. J. Mortimer, G. D. Wilcox, A. M. Teridi, T. S. Varley and K. G. U. Wijayantha, *et al.*, Electrochromic and Colorimetric Properties of Nickel(II) Oxide Thin Films Prepared by Aerosol-Assisted Chemical Vapor Deposition, *ACS Appl. Mater. Interfaces*, 2013, **5**(12), 5675–5682, DOI: 10.1021/am401025v.

37 I. Bouessay, A. Rougier, P. Poizot, J. Moscovici, A. Michalowicz and J. M. Tarascon, Electrochromic degradation in nickel oxide thin film: A self-discharge and dissolution phenomenon, *Electrochim. Acta*, 2005, **50**(18), 3737–3745. Available from: https://www.sciencedirect.com/science/article/pii/S0013468605000721.

38 Y. Ren, W. K. Chim, L. Guo, H. Tanoto, J. Pan and S. Y. Chiam, The coloration and degradation mechanisms of electrochromic nickel oxide, *Sol. Energy Mater. Sol. Cells*, 2013, **116**, 83–88. Available from: https://www.sciencedirect.com/science/article/pii/S0927024813001633.

39 T. Hisatomi, J. Kubota and K. Domen, Recent advances in semiconductors for photocatalytic and photoelectrochemical water splitting, *Chem. Soc. Rev.*, 2014, **43**(22), 7520–7535, DOI: 10.1039/C3CS60378D.

40 A. Czapla, E. Kusior and M. Bucko, Optical properties of non-stoichiometric tin oxide films obtained by reactive sputtering, *Thin Solid Films*, 1989, **182**(1), 15–22. Available from: https://www.sciencedirect.com/science/article/pii/0040609089902393.

41 R. Merlin, Electronic Structure of NiO, *Phys. Rev. Lett.*, 1985, **54**(25), 2727. Available from: https://link.aps.org/doi/10.1103/PhysRevLett.54.2727.

42 S. Haghverdi Khamene, C. van Helvoirt, M. N. Tsampas and M. Creatore, Electrochemical Activation of Atomic-Layer-Deposited Nickel Oxide for Water Oxidation, *J. Phys. Chem. C*, 2023, **127**(46), 22570–22582, DOI: 10.1021/acs.jpcc.3c05002.

43 J. Noguera-Gómez, M. García-Tecedor, J. F. Sánchez-Royo, L. M. Valencia Liñán, M. de la Mata and M. Herrera-Collado, *et al.*, Solution-Processed Ni-Based Nanocomposite Electrocatalysts: An Approach to Highly Efficient Electrochemical Water Splitting, *ACS Appl. Energy Mater.*, 2021, **4**(5), 5255–5264, DOI: 10.1021/acsaem.1c00776.

44 M. Awais, D. D. Dowling, F. Decker and D. Dini, Photoelectrochemical properties of mesoporous NiOx deposited on

894 | *Energy Environ. Sci.*, 2026, **19**, 884–895

This journal is © The Royal Society of Chemistry 2026

technical FTO via nanopowder sintering in conventional and plasma atmospheres, *SpringerPlus*, 2015, **4**(1), 564, DOI: 10.1186/s40064-015-1265-3.

45 L. D. Kadam and P. S. Patil, Studies on electrochromic properties of nickel oxide thin films prepared by spray pyrolysis technique, *Sol. Energy Mater. Sol. Cells*, 2001, **69**(4), 361–369. Available from: https://www.sciencedirect.com/science/article/pii/S0927024800004037.

46 G. Boschloo and A. Hagfeldt, Spectroelectrochemistry of Nanostructured NiO, *J. Phys. Chem. B*, 2001, **105**(15), 3039–3044, DOI: 10.1021/jp003499s.

47 T. Ivanova, A. Harizanova, M. Shipochka and P. Vitanov, Nickel Oxide Films Deposited by Sol-Gel Method: Effect of Annealing Temperature on Structural, Optical, and Electrical Properties, *Materials*, 2022, **15**(5), 1742, DOI: 10.3390/ma15051742.

48 P. Horak, V. Lavrentiev, V. Bejsovec, J. Vacik, S. Danis and M. Vrnata, *et al.*, Study of structural and electrical properties of thin NiOx films prepared by ion beam sputtering of Ni and subsequent thermo-oxidation, *Eur. Phys. J. B*, 2013, **86**(11), 470, DOI: 10.1140/epjb/e2013-30969-6.

49 M. C. Biesinger, B. P. Payne, L. W. M. Lau, A. Gerson and R. S. C. Smart, X-ray photoelectron spectroscopic chemical state quantification of mixed nickel metal, oxide and hydroxide systems, *Surf. Interface Anal.*, 2009, **41**(4), 324–332, DOI: 10.1002/sia.3026.

50 A. Al-Ashouri, E. Köhnen, B. Li, A. Magomedov, H. Hempel and P. Caprioglio, *et al.*, Monolithic perovskite/silicon tandem solar cell with >29% efficiency by enhanced hole extraction, *Science*, 2020, **370**(6522), 1300–1309, DOI: 10.1126/science.abd4016.

51 Z. Li, X. Sun, X. Zheng, B. Li, D. Gao and S. Zhang, *et al.*, Stabilized hole-selective layer for high-performance inverted p-i-n perovskite solar cells, *Science*, 2023, **382**(6668), 284–289, DOI: 10.1126/science.ade9637.

52 T. Wang, Z. Wang, Z. Ma, J. Kang, Z. Wang and X. Zong, *et al.*, Boosting interfacial contact for the NiOx-based inverted perovskite solar cells via D-A type semiconductor, *Chem. Eng. J.*, 2024, **496**, 154011. Available from: https://www.sciencedirect.com/science/article/pii/S1385894724055001.

53 N. Phung, M. Verheijen, A. Todinova, K. Datta, M. Verhage and A. Al-Ashouri, *et al.*, Enhanced Self-Assembled Monolayer Surface Coverage by ALD NiO in p-i-n Perovskite Solar Cells, *ACS Appl. Mater. Interfaces*, 2022, **14**(1), 2166–2176, DOI: 10.1021/acsami.1c15860.

54 T. Nie, Z. Fang, J. Ding and S. Liu, Improving the efficiency and stability of nickel oxide perovskite solar cells with doping and surface treatment strategies, *Device*, 2024, **2**(10), 100498. Available from: https://www.sciencedirect.com/science/article/pii/S2666998624003946.

55 J. M. Luther, M. Law, Q. Song, C. L. Perkins, M. C. Beard and A. J. Nozik, Structural, Optical, and Electrical Properties of Self-Assembled Films of PbSe Nanocrystals Treated with 1,2-Ethanedithiol, *ACS Nano*, 2008, **2**(2), 271–280, DOI: 10.1021/nn7003348.

56 Q. Lian, K. Wang, K. Feng, B. Li, B. Li and S. Gámez-Valenzuela, *et al.*, Tuning NiOx/Perovskite Heterointerface via Synergistic Molecular Design Strategy of Carbazole Phosphonic Acid for High-Performance Inverted Perovskite Solar Cells, *Adv. Funct. Mater.*, 2025, **35**(46), 2506315, DOI: 10.1002/adfm.202506315.

57 J. F. Ambrose and R. F. Nelson, Anodic Oxidation Pathways of Carbazoles: I. Carbazole and N-Substituted Derivatives, *J. Electrochem. Soc.*, 1968, **115**(11), 1159, DOI: 10.1149/1.2410929.

58 J. F. Ambrose and R. F. Nelson, Anodic oxidation pathways of carbazoles: I. carbazole and N-substituted derivatives, *J. Electrochem. Soc.*, 1968, **115**(11), 1159.

59 A. S. Saraç and E. Sezer, Electro-induced oxidative polymerization of N-vinylcarbazole, *Polym. Adv. Technol.*, 1999, **10**(3), 135–140, DOI: 10.1002/(SICI)1099-1581(199903)10:3<135::AID-PAT852>3.0.CO;2-H.

60 C. Wang, L. Ouyang, X. Xu, S. Braun, X. Liu and M. Fahlman, Relationship of Ionization Potential and Oxidation Potential of Organic Semiconductor Films Used in Photovoltaics, *Sol. RRL*, 2018, **2**(9), 1800122, DOI: 10.1002/solr.201800122.

61 W. Peng, Y. Zhang, X. Zhou, J. Wu, D. Wang and G. Qu, *et al.*, A versatile energy-level-tunable hole-transport layer for multi-composition inverted perovskite solar cells, *Energy Environ. Sci.*, 2025, **18**(2), 874–883, DOI: 10.1039/D4EE03208J.

62 F. J. Angus, W. K. Yiu, H. Mo, T. L. Leung, M. U. Ali and Y. Li, *et al.*, Understanding the Impact of SAM Fermi Levels on High Efficiency p-i-n Perovskite Solar Cells, *J. Phys. Chem. Lett.*, 2024, **15**(42), 10686–10695, DOI: 10.1021/acs.jpclett.4c02345.

63 W. Jiang, F. Li, M. Li, F. Qi, F. R. Lin and A. K. Y. Jen, π-Expanded Carbazoles as Hole-Selective Self-Assembled Monolayers for High-Performance Perovskite Solar Cells, *Angew. Chem., Int. Ed.*, 2022, **61**(51), e202213560, DOI: 10.1002/anie.202213560.

This journal is © The Royal Society of Chemistry 2026

Energy Environ. Sci., 2026, **19**, 884–895 | **895**